Med Biol Eng Comput (2013) 51:513–523
DOI 10.1007/s11517-012-1019-0

ORIGINAL ARTICLE

Atherosclerotic plaque tissue characterization in 2D ultrasound longitudinal carotid scans for automated classification: a paradigm for stroke risk assessment

U. Rajendra Acharya · Muthu Rama Krishnan Mookiah · S. Vinitha Sree · David Afonso · Joao Sanches · Shoaib Shafique · Andrew Nicolaides · L. M. Pedro · J. Fernandes e Fernandes · Jasjit S. Suri

Received: 15 February 2012 / Accepted: 17 December 2012 / Published online: 6 January 2013

Abstract In the case of carotid atherosclerosis, to avoid unnecessary surgeries in asymptomatic patients, it is necessary to develop a technique to effectively differentiate symptomatic and asymptomatic plaques. In this paper, we have presented a data mining framework that characterizes the textural differences in these two classes using several grayscale features based on a novel combination of trace transform and fuzzy texture. The features extracted from the delineated plaque regions in B-mode ultrasound images were used to train several classifiers in order to prepare them for classification of new test plaques. Our CAD system was evaluated using two different databases consisting of 146 (44 symptomatic to 102 asymptomatic) and 346 (196 symptomatic and 150 asymptomatic) images. Both these databases differ in the way the ground truth was determined. We obtained classification accuracies of 93.1 and 85.3 %, respectively. The techniques are low cost, easily implementable, objective, and non-invasive. For more objective analysis, we have also developed novel integrated indices using a combination of significant features.

Keywords Atherosclerosis · Carotid ultrasound · Classification · Fuzzy texture · Index · Plaque characterization · Trace transform

U. R. Acharya · M. R. K. Mookiah
Department of Electronics and Computer Engineering, Ngee Ann Polytechnic, Clementi, Singapore
e-mail: aru@np.edu.sg

M. R. K. Mookiah
e-mail: mkm2@np.edu.sg

U. R. Acharya
Department of Biomedical Engineering, Faculty of Engineering, University of Malaya, Kuala Lumpur, Malaysia

S. Vinitha Sree (✉) · J. S. Suri
Global Biomedical Technologies Inc., CA, USA
e-mail: vinitha.sree@gmail.com

D. Afonso · J. Sanches
Department of Electrical and Computer Engineering, Instituto Superior Tecnico, Lisbon, Portugal
e-mail: dafonso@isr.ist.utl.pt

J. Sanches
e-mail: jmrs@isr.ist.utl.pt

S. Shafique
CorVasc MDs, Indianapolis, IN, USA
e-mail: sshafiqu@iupui.edu

A. Nicolaides
Vascular Screening and Diagnostic Centre, London, Imperial college, London, UK
e-mail: a.nicolaides@imperial.ac.uk

A. Nicolaides
Department of Biological Sciences, University of Cyprus, Nicosia, Cyprus

L. M. Pedro · J. Fernandes e Fernandes
Cardiovascular Institute and the Lisbon University Medical School, Hospital de SantaMaria, 1600-190 Lisbon, Portugal
e-mail: lmendespedro@clix.pt

J. Fernandes e Fernandes
e-mail: jff@me.com

J. S. Suri
Department of Biomedical Engineering, Idaho State University, Pocatello, ID, USA
e-mail: jsuri@comcast.net

J. S. Suri
Diagnostic and Monitoring Division, AtheroPoint(TM) LLC Roseville, CA, USA

1 Introduction

Carotid atherosclerosis is a degenerative disease resulting in the formation of plaques in the carotid arteries [10] and can lead to stroke. The World Health Organization estimates that by 2030, almost 23.6 million people will die mostly from heart disease and stroke [39]. Plaque rupture was seen in 74 % of symptomatic plaques (*Sym*) and in only 32 % of asymptomatic (*Asym*) plaques [9]. Since there is a considerable risk for the patient undergoing either carotid artery stenting (CAS) or carotid endarterectomy (CEA) [8], only those symptomatic patients at risk of stroke should be offered these procedures. When the degree of stenosis (DoS) based on European carotid surgery trial (ESCT) criteria was greater than 80 %, CEA was prescribed [15]. However, there is evidence that plaques with relatively low stenosis degree may produce symptoms [29] and the majority of asymptomatic patients with highly stenotic atherosclerotic plaques remain asymptomatic [21]. Therefore, there is a need for efficient plaque characterization techniques that can detect *Sym* and *Asym* groups.

The common carotid artery (CCA) is examined to detect the presence of plaques in the carotid artery [16]. The preferred modality is non-invasive ultrasound in view of its low cost and availability. Ultrasound-based interpretations are limited by the need for experienced ultrasonographers, low image resolution, and image artifacts. Computer aided diagnostic (CAD) techniques can address these issues [36]. It was observed that plaque echogenicity from B-mode ultrasound images could be used for *Sym* versus *Asym* classification [18]. Several studies addressed the automated segmentation of carotid plaque using ultrasound images [2, 3, 30]. Gray Scale Median values, used for quantitative estimation of echogenicity, have been found to be low for the *Sym* group [13]. Several studies have hence developed CAD tools that utilize features quantifying the grayscale changes in *Sym* and *Asym* images for plaque classification [2, 3, 6, 11, 24, 25, 27, 34]. Such CAD tools use extracted significant features from plaque images to train classifiers which can then predict if an unknown-class image most likely belongs to the *Sym* or *Asym* group. The ground truth of whether a plaque is *Sym* or *Asym* is based on the prior history of symptoms. Our study protocol is in line with other related studies [2, 3, 6, 11, 24, 25, 27, 34] (as shown in Sect. 7).

In this work, we have developed CAD techniques for two plaque datasets (called as UK and Portugal). The Portugal dataset has plaques that are confirmed *Sym* or *Asym* based on longitudinal studies. The UK dataset was obtained in a cross-sectional study, and hence, some *Asym* plaques may have the characteristics of *Sym* plaques if they were imaged while they were progressing towards the *Sym* type. We chose these two datasets to demonstrate the effect of the ground truth (based on the clinical symptoms) on the classification accuracies. Thus, the objectives of this work were (1) to develop a tissue characterization data mining framework to classify plaques into *Sym* and *Asym* types, (2) to demonstrate the importance of valid ground truth based on patient's clinical symptoms, and (3) to develop integrated indices using grayscale features whose range can be used to more objectively, easily, and quickly classify plaques.

The proposed CAD system consists of an off-line training system depicted by all the blocks outside the dotted shaded rectangular box in Fig. 1 and an on-line real-time system depicted by all the blocks within the shaded rectangular box. In the off-line system, the training images are pre-processed and manually segmented, and grayscale features are extracted from plaque regions, based on combination of trace transform and fuzzy texture. Further, significant features are selected. These features and the ground truth are used to train several supervised learning-based classifiers. The output of this off-line training system is the training parameters for each classifier. These off-line training parameters are then used to transform the feature

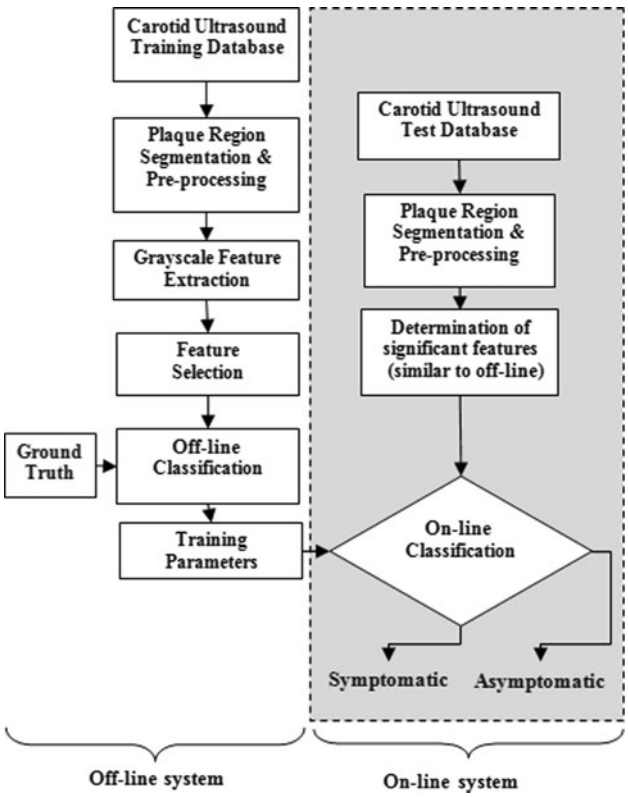

Fig. 1 Block diagram of the proposed CAD technique for plaque characterization. The blocks outside the *dotted shaded rectangular box* represent the flow in the off-line training system, and the blocks within the *dotted box* indicate the on-line system

vectors estimated on-line from a test image to determine its class. This predicted class is compared with the ground truth class to obtain the performance measures like accuracy, sensitivity, specificity, and positive predictive value (PPV).

The information in this paper is organized as follows. In Sect. 2, we describe the datasets used, and we present the feature extraction and selection techniques in Sect. 3 and classification methodology in Sect. 4. The integrated indices are described in Sect. 5, and the selected features and classification results are presented in Sect. 6. Section 7 includes a discussion on the results, and presents the features and limitations of our proposed technique. We conclude the paper in Sect. 8.

2 Description of data

For both datasets, approval from Institutional Review Board and ethics committee and consent from patients were obtained prior to the study.

2.1 Portugal dataset

In the literature, there are studies that have collected multiple views of the same anatomy to increase the sample size [32], and hence, we have obtained 146 carotid bifurcation plaque images from 99 patients (75 males and 24 females; 102 *Asym* and 44 *Sym*; mean age: 68.) The data collection was done at Instituo Cardiovascular de Lisboa in Lisbon, Portugal. A plaque was considered *Sym* when the subject experienced Amaurosis Fugax (AF) or focal transitory, reversible or established neurological symptoms in the ipsilateral carotid territory in the previous 6 months. If there were no symptoms, the plaque was considered Asym.

Patients were selected consecutively through neurological consultation which included non-invasive examination with color-flow duplex scan of one or both carotids. HDI5000 Philips machine, with a L12-5 scan probe with 5–12 MHz broadband linear array transducer operating in B-mode, was used for image acquisition. The images were sampled at a density of 25 pixels/mm. Image normalization was carried out [13] and the intensities of the normalized image were linearly scaled so that the adventitia and blood intensities would be in the range of 190–195 and 0–5, respectively. The normalized image was used to segment the plaque region(s) of interest (ROI) in the image. The medical practitioner delineated the plaque by drawing around its structure. The resultant contour was evenly resampled and smoothed using spline interpolation. Matlab software was used for normalization and ROI selection. Figure 2 shows typical *Sym* and *Asym* carotid images, their corresponding Color Doppler images, and the respective zoomed ROIs.

2.2 UK dataset

This set consisted of 346 images (150 *Asym* and 196 *Sym*) collected from patients (mean age ± SD: 69.9 ± 7.8; 61 % male) referred to the Saint Mary's Hospital, UK for diagnostic carotid ultrasound. The plaques from subjects who had retinal or hemispheric symptoms such as stroke, transient ischemic attack (TIA), and AF in the previous 6 months were classified as *Sym*. Asymptomatic patients were referred because of hyperlipidemia, the presence of a cervical bruit, or for screening prior to cardiac surgery. Subjects with cardioembolic symptoms or distant symptoms (>6 months)

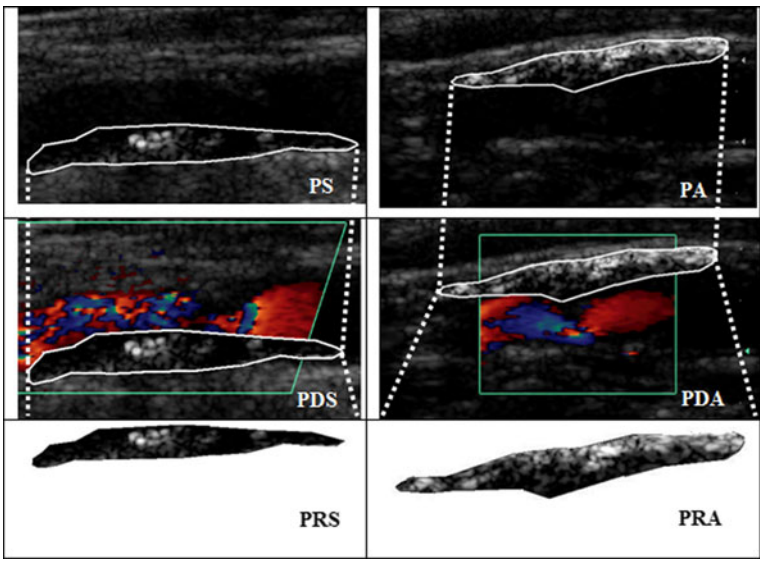

Fig. 2 Portugal dataset. Carotid symptomatic plaque (PS) and asymptomatic (PA) images; corresponding color Doppler images (PDS and PDA); corresponding extracted plaque region of interests (Zoomed) (PRS and PRA)

were eliminated. Surgery was found to be highly beneficial for plaques with 70–99 % DoS and moderately beneficial for 50–69 % degree [33]. Therefore, we included plaques with greater than 50 % DoS.

The ultrasonographers who acquired the plaque images knew the reason for referral, as they performed routine diagnostic testing. However, the persons who subsequently did the image normalization and analysis were blind to the class of the plaques. The ultrasound images were acquired used a standard image acquisition procedure [26] using an ATL HDI 3000 duplex scanner with a linear broadband width 4–7 MHz (multi-frequency) transducer. The images were sampled at a density of 20 pixels/mm. The Plaque Texture Analysis software [19] was used for normalization and plaque ROI selection. Post-normalization, the median gray level intensity of blood was in the range of 0–5 and that of adventitia layer was in the range of 180–190. To select the plaque ROI, medical practitioners outlined the plaque with the mouse and saved it as a new file. Figure 3 shows typical *Sym* and *Asym* carotid images, their corresponding Color Doppler images, and the respective zoomed ROIs.

3 Grayscale feature extraction and selection

In the ultrasound images, plaques are characterized by echodensity (homogeneous and heterogeneous). Studies have shown that patients with hypoechoic [29] and heterogeneous plaques [1] will be at an increased risk of future stroke. These variations in the echodensity level can be captured using texture features which quantify the pixel intensity variations in the image.

3.1 Trace transform

The acquired ultrasound images may be slightly different due to various acquisition angles and gain settings. Trace transform allows us to extract features that are invariant to transformations like rotation, translation, and scaling. In this method, the Trace Transform Matrix is first obtained by applying a trace functional T along line tracing the input image. Here, the image is transformed to a $(\phi; p; t)$parameter space. Then, a diametric functional P is applied along the columns of the trace transform matrix (p direction) to get a string. Finally, a circus functional Φ is applied along the string (ϕ direction) to obtain a single number feature, called the triple feature [23]. p is the distance of the centre of the image from the tracing line. The value of the p chosen in this work is 2. The value of the circus function Φ varies from 1° to 180°. t is the sampling intervals of tracing lines. In this work, we have chosen $t = 0.5$. Thus, the triple feature $\Pi(f, I)$of image $f(x,y)$ in image space I can be defined as

$$\Pi(f, I) = \Phi(P(T(f(I; p, \phi, t)))). \quad (1)$$

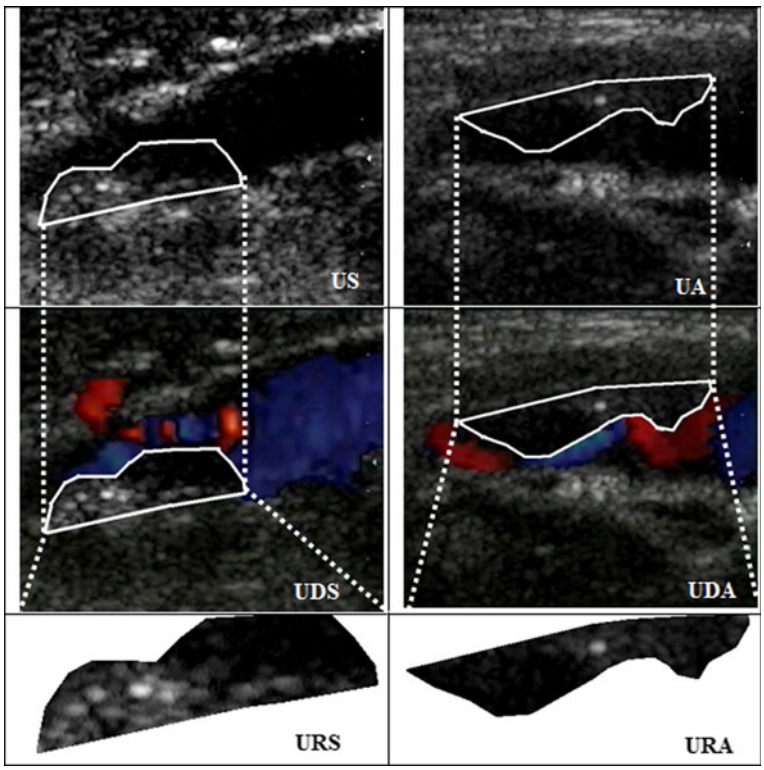

Fig. 3 UK dataset: carotid symptomatic (US) and asymptomatic (UA) images; corresponding color Doppler images (UDS and UDA); corresponding extracted plaque region of interests (Zoomed) (URS and URA)

In this work, we calculated two triple features (2) and (3) using the invariant functionals IF_1, IF_2, and IF_3 defined in [23].

$$\Pi_1 = (T \rightarrow \mathrm{IF}_1, P \rightarrow \mathrm{IF}_2, \Phi \rightarrow \mathrm{IF}_3) \quad (2)$$

$$\Pi_2 = (T \rightarrow IF_3, P \rightarrow IF_2, \Phi \rightarrow IF_1) \quad (3)$$

where $\Pi_1$is the normalized version of the triple feature formed by using IF_1, IF_2, and IF_3 for functionals T, P, and Φ, respectively in (1). $\Pi_2$uses IF_3, IF_2,and IF_1 for functionals T, P, and Φ, respectively.

3.2 Fuzzy gray level co-occurrence matrix (FGLCM)

Typically, there are no crisp boundaries separating the various regions in an image. Hence, we used fuzzy-logic based features in this work. Gray level co-occurrence matrix (GLCM) is made up of the frequency of appearance of a gray level in a specified linear relationship with another gray level within the neighborhood of interest. The FGLCM [22] of an image I of size $L \times L$ is given by

$$F_d(m,n) = [f_{mn}]_{L\times L} \quad (4)$$

where f_{mn} corresponds to the frequency of occurrence of a gray value 'around m' separated from another pixel, with gray value 'around n', by a distance d in a specific direction θ. In this study, we used rotational invariant co-occurrence matrix F_d, obtained by averaging the four symmetrical fuzzy co-occurrence matrices computed with $\theta = 0^\circ$, 45°, 90°, 135° and $d = 20$. The following FGLCM-based features were obtained:

$$\text{Energy} : E_{\text{fuzzy}} = \sum_m \sum_n [F_d(m,n)]^2 \quad (5)$$

$$\text{Contrast} : C_{\text{fuzzy}} = \sum_m \sum_n (m-n)^2 F_d(m,n) \quad (6)$$

$$\text{Homogeneity} : G_{\text{fuzzy}} = \sum_m \sum_n \frac{F_d(m,n)}{1+(m-n)^2} \quad (7)$$

$$\text{Entropy} : H_{\text{fuzzy}} = -\sum_m \sum_n F_d(m,n) \ln F_d(m,n) \quad (8)$$

$$\text{Correlation} : \text{Corr}_{\text{fuzzy}} = \sum_m \sum_n [mnF_d(m,n)] - \mu_m\mu_n/\sigma_m\sigma_n \quad (9)$$

where

$$\mu_m = \sum mF_d(m,n), \quad \sigma_m^2 = \sum m^2F_d(m,n) - \mu_m^2 \quad (10)$$

$$\mu_n = \sum nF_d(m,n), \quad \sigma_n^2 = \sum n^2F_d(m,n) - \mu_n^2 \quad (11)$$

Moments M_1, M_2, M_3, and M_4:

$$M^g_{\text{fuzzy}} = \sum_m \sum_n (m-n)^g F_d(m,n). \quad (12)$$

The similarity between two pixels that are $(\Delta m, \Delta n)$ apart is measured by the homogeneity feature and the local variation between those two pixels is captured by the contrast feature. The density and the degree of disorder are measured by energy and entropy features. Maximum entropy is achieved when all elements of the co-occurrence matrix are the same.

Difference statistics is defined as "the distribution of the probability that the gray-level difference is k between the points separated by δ in an image" [37]. The difference statistics vector can be obtained from FGLCM as [37]

$$F_\delta(k) = \sum_{\substack{m \\ |m-n|=k}} \sum_n F_d(m,n) \quad (13)$$

where $k = 0, 1, \ldots c-1$, c is the number of grayscale levels [14], and δ is $d = (\Delta m, \Delta n)$. Based on the acquired vector, we obtain the following difference statistics-based features [38]:

$$\text{Angular second moment} : \text{ASM}_{\text{diff}} = \sum_{k-0}^{c-1} F_\delta(k)^2 \quad (14)$$

$$\text{Mean} : \mu_{\text{diff}} = \sum_{k-0}^{c-1} kF_\delta(k) \quad (15)$$

$$\text{Contrast} : C_{\text{diff}} = \sum_{k-0}^{c-1} k^2F_\delta(k) \quad (16)$$

$$\text{Entropy} : H_{\text{diff}} = -\sum_{k-0}^{c-1} F_\delta(k) \log F_\delta(k) \quad (17)$$

When the $F_\delta(k)$ values are very similar, ASM is small. When $F_\delta(k)$ values are concentrated near the origin, mean is small. Entropy is largest when $F_\delta(k)$ values are equal. The above-mentioned features were calculated for $\delta = (0, 1)$, $(1, 1)$, and $(1, 0)$, and the mean values for the four features were taken.

The FGLCM contains information about the positions of pixels having similar gray level values. However, the difference statistics-based features are derived from the vector based on absolute differences between pairs of gray levels. Thus, even though the definitions of features like contrast [(6) and (16)] and entropy [(8) and (17)] are similar, they are calculated on different matrices/vectors that quantify the texture of the image in different ways.

3.3 Fuzzy run length matrix (FRLM)

The run length matrix, $F_\theta(m,n)$, consists of the number of elements where gray level value i has the run length j continuous in direction θ [17]. Often the direction θ is set as 0°, 45°, 90°, and 135°. The features listed below were calculated for analysis and classification:

Short run emphasis : $\mathrm{SRE}_{\mathrm{fuzzy}}$

$$= \sum_m \sum_n \frac{F_\theta(m,n)}{n^2} \Bigg/ \sum_m \sum_n F_\theta(m,n) \tag{18}$$

Long run emphasis : $\mathrm{LRE}_{\mathrm{fuzzy}}$

$$= \sum_m \sum_n n^2 F_\theta(m,n) \Bigg/ \sum_m \sum_n F_\theta(m,n) \tag{19}$$

Gray level non - uniformity : $\mathrm{GLNU}_{\mathrm{fuzzy}}$

$$= \sum_m \left\{ \sum_n F_\theta(m,n) \right\}^2 \Bigg/ \sum_m \sum_n F_\theta(m,n) \tag{20}$$

Run length non - uniformity : $\mathrm{RLNU}_{\mathrm{fuzzy}}$

$$= \sum_n \left\{ \sum_m F_\theta(m,n) \right\}^2 \Bigg/ \sum_m \sum_n F_\theta(m,n) \tag{21}$$

Run percentage : $\mathrm{RP}_{\mathrm{fuzzy}} = \sum_m \sum_n F_\theta(m,n) \Big/ A$ (22)

where A is the area of the image of interest.

3.4 Feature selection

We tested the UK and Portugal dataset-based features using Q–Q plot and Kolmogorov–Smirnov test to check whether the features had normal distribution. Since they were normally distributed, we used the Student's t test to assess whether the means of a feature from two classes are significantly different [7]. We observed that all the features had a normal distribution, which is a necessary condition for applying the t test.

4 Classification

The objective of a data mining technique is to determine the optimal combination of feature set and classifier that gives the best classification accuracy. We have, therefore, evaluated some of the most commonly used classifiers, namely, support vector machine (SVM), gaussian mixture model (GMM), radial basis probabilistic neural network (RBPNN), decision tree (DT), k-nearest neighbor (KNN), Naïve Bayes classifier (NBC), and fuzzy classifier, in this work. We used stratified threefold cross validation data resampling technique to evaluate the classifiers. In this technique, the dataset is randomly split into three equal parts. Two parts are used for training the classifiers that yield the training parameters. During the testing phase, these training parameters are used on the remaining one part, and the resultant class labels are used to calculate accuracy, sensitivity, specificity, and PPV. This process is repeated two more times, using a different part for testing each time, ensuring that no test image is in the training set. The average of the performance measures (sensitivity, specificity, accuracy, and PPV) obtained over all the three folds are reported as the final performance measures.

We describe only those classifiers that presented the highest accuracies. The objective of SVM classifier is to find a separating hyperplane that separates the training samples belonging to the two classes with a maximum margin between the hyperplane and the sample closest to the hyperplane [12]. In the case of nonlinearly separable data, kernel functions are used to map the original feature space to a higher dimensional feature space where the features become linearly separable [28]. The polynomial kernels of varying orders and the radial basis function (RBF) kernels have been used in this work. The NBC is a simple probabilistic classifier which works on the assumption that the features are independent. Class prior probabilities and feature probability distributions used in the Naive Bayes model are determined from the training set using maximum likelihood algorithm. This model is then used along with a maximum a posteriori decision rule to determine the class label of new test samples [20]. In the case of fuzzy classifier, a subtractive clustering technique is used to generate a fuzzy inference system [31], which contains set of fuzzy rules which are used to perform fuzzy inference calculations of the test data. In this work, we used the Sugeno technique [35].

5 Clinical indices for screening

Tables 1 and 2, in the next section, indicate the number of significant features for the Portugal and UK datasets, respectively. It would be difficult to individually keep track of the variations in each of the features. Therefore, for each dataset, we have empirically determined a single integrated index that is a unique combination of the respective features that results in a unique range for both the classes. These non-dimensional indices can be more comprehendible to the physicians than the classifiers which are most times black boxes that directly output the class label. When continuously monitored, the variations in the indices can throw light on how the asymptomatic plaques become symptomatic over time. *PlaqueindexP*, given by (23), was calculated using the features in Table 1. Here, the value of χ_P was taken to be 35. *PlaqueindexU*, given by (26), was calculated using the features in Table 2. The value of χ_U was taken to be -10.

$$PlaqueindexP = \frac{\alpha_P}{\beta_P(-1 \times 10^{\chi_P})} \tag{23}$$

Table 1 Portugal dataset: range (mean ± standard deviation) of the significant features that had a p value less than 0.05

Feature	Symptomatic	Asymptomatic	p value
$\prod_1(P)$	3.08 ± 0.43	2.72 ± 0.40	<0.0001
$\prod_2(P)$	$1.04 \times 10^{03} \pm 3.34 \times 10^{02}$	$1.19 \times 10^{03} \pm 2.83 \times 10^{02}$	0.0034
$E_{\text{fuzzy}}(P)$	$2.03 \times 10^{05} \pm 1.39 \times 10^{05}$	$2.75 \times 10^{05} \pm 1.94 \times 10^{05}$	0.0193
$C_{\text{fuzzy}}(P)$	72.89 ± 13.11	66.85 ± 15.39	0.0171
$M^2_{\text{fuzzy}}(P)$	$1.80 \times 10^{04} \pm 3.32 \times 10^{03}$	$1.65 \times 10^{04} \pm 3.91 \times 10^{03}$	0.0170
$M^4_{\text{fuzzy}}(P)$	$1.15 \times 10^{09} \pm 2.11 \times 10^{08}$	$1.05 \times 10^{09} \pm 2.48 \times 10^{08}$	0.0170
$\text{ASM}_{\text{diff}}(P)$	$3.57 \times 10^{07} \pm 4.82 \times 10^{07}$	$6.71 \times 10^{07} \pm 8.68 \times 10^{07}$	0.0181
$C_{\text{diff}}(P)$	$8.48 \times 10^{05} \pm 4.19 \times 10^{05}$	$1.01 \times 10^{06} \pm 4.28 \times 10^{05}$	0.0253
$\mu_{\text{diff}}(P)$	$3.43 \times 10^{03} \pm 1.70 \times 10^{03}$	$4.10 \times 10^{03} \pm 1.76 \times 10^{03}$	0.0237
$\text{H}_{\text{diff}}(P)$	−39.96 ± 38.72	−64.26 ± 58.07	0.0077
$\text{LRE}_{\text{fuzzy}}(P)$	56.02 ± 46.10	97.68 ± 136.51	0.0372
$\text{RLNU}_{\text{fuzzy}}(P)$	$4.20 \times 10^{02} \pm 1.72 \times 10^{02}$	$3.54 \times 10^{02} \pm 1.31 \times 10^{03}$	0.0092

Table 2 UK dataset: range (mean ± standard deviation) of the significant features that had a p value less than 0.05

Feature	Symptomatic	Asymptomatic	p value
$\prod_1(U)$	3.41 ± 0.66	3.80 ± 0.59	<0.0001
$\prod_2(U)$	$9.36 \times 10^{02} \pm 3.40 \times 10^{03}$	$1.09 \times 10^{03} \pm 3.98 \times 10^{02}$	<0.0001
$G_{\text{fuzzy}}(U)$	0.48 ± 0.06	0.55 ± 0.08	<0.0001
$H_{\text{fuzzy}}(U)$	1.53 ± 0.15	1.32 ± 0.22	<0.0001
$C_{\text{fuzzy}}(U)$	63.41 ± 18.39	40.86 ± 26.23	<0.0001
$\text{Corr}_{\text{fuzzy}}(U)$	0.01 ± 0.00	0.01 ± 0.00	<0.0001
$M^2_{\text{fuzzy}}(U)v$	$1.57 \times 10^{04} \pm 4.65 \times 10^{03}$	$10 \times 10^{03} \pm 6.63 \times 10^{03}$	<0.0001
$M^4_{\text{fuzzy}}(U)$	$9.97 \times 10^{08} \pm 2.95 \times 10^{08}$	$6.35 \times 10^{08} \pm 4.21 \times 10^{08}$	<0.0001
$\text{ASM}_{\text{diff}}(U)$	$8.68 \times 10^{07} \pm 1.43 \times 10^{08}$	$5.23 \times 10^{07} \pm 7.30 \times 10^{07}$	0.0071
$C_{\text{diff}}(U)$	$1.01 \times 10^{06} \pm 6.44 \times 10^{05}$	$5.25 \times 10^{05} \pm 5.29 \times 10^{05}$	<0.0001
$\mu_{\text{diff}}(U)$	$4.09 \times 10^{03} \pm 2.60 \times 10^{03}$	$2.15 \times 10^{03} \pm 2.12 \times 10^{03}$	<0.0001
$H_{\text{diff}}(\text{U})$	−69.08 ± 72.65	−46.85 ± 45.99	0.0011
$\text{SRE}_{\text{fuzzy}}(U)$	0.58 ± 0.22	0.87 ± 0.03	<0.0001
$\text{LRE}_{\text{fuzzy}}(U)$	242.07 ± 277.69	39.50 ± 31.53	<0.0001
$\text{RP}_{\text{fuzzy}}(U)$	0.33 ± 0.25	0.62 ± 0.26	<0.0001
$\text{GLNU}_{\text{fuzzy}}(U)$	$5.03 \times 10^{03} \pm 7.40 \times 10^{03}$	$1.08 \times 10^{04} \pm 6.91 \times 10^{03}$	<0.0001

where

$$\alpha_P = E_{\text{fuzzy}}(P) \times C_{\text{fuzzy}}(P) \times M^2_{\text{fuzzy}}(P) \times M^4_{\text{fuzzy}}(P) \times \text{ASM}_{\text{diff}}(P) \times C_{\text{diff}}(P) \times \mu_{\text{diff}}(P) \times H_{\text{diff}}(P) \times \text{LRE}_{\text{fuzzy}}(P) \times \text{RLNU}_{\text{fuzzy}}(P) \quad (24)$$

$$\beta_P = \prod_1(P) \times \prod_2(P) \quad (25)$$

$$PlaqueindexU = \frac{\alpha_U}{\beta_U(-1 \times 10^{\chi_U})} \quad (26)$$

where

$$\alpha_U = G_{\text{fuzzy}}(U) \times H_{\text{fuzzy}}(U) \times C_{\text{fuzzy}}(U) \times \text{Corr}_{\text{fuzzy}}(U) \times \text{ASM}_{\text{diff}}(U) \times C_{\text{diff}}(U) \times \mu_{\text{diff}}(U) \times H_{\text{diff}}(U) \times \text{SRE}_{\text{fuzzy}}(U) \times \text{LRE}_{\text{fuzzy}}(U) \times \text{RP}_{\text{fuzzy}}(U) \times \text{GLNU}_{\text{fuzzy}}(U) \times \text{RLNU}_{\text{fuzzy}}(U) \quad (27)$$

$$\beta_U = \prod_1(U) \times \prod_2(U) \times M^2_{\text{fuzzy}}(U) \times M^4_{\text{fuzzy}}(U). \quad (28)$$

6 Results

6.1 Selected features

Table 1 presents the significant features obtained for the Portugal dataset [indicated as feature(P)] and Table 2 for the UK dataset [indicated as feature(U)]. It is evident that all the features have p values less than 0.05 deeming them significant. In both tables, no single feature is distinctively, highly different between the two classes. This implies that a combination of these features have to be used for training the classifiers. Moreover, between the two datasets, there is no uniformity in the feature variations. For instance,

$C_{diff}(P)$ is higher for symptomatic plaques and $C_{diff}(U)$ is higher for asymptomatic plaques. Such nonuniformity reflects the difference in the plaques recorded in both datasets. The reason for this difference is given at the end of this section.

6.2 Classification results

Table 3 presents the classification results obtained using both the datasets. To develop a classification framework for the UK dataset, the classifiers were trained with data from the UK dataset only. Similar is the case for the Portugal dataset. In the case of the Portugal dataset, the fuzzy classifier was chosen as the optimal classifier as it not only presents the highest accuracy of 93.1 % but also has equally good sensitivity of 99.0 % and specificity of 80 %. In the case of the UK dataset, the highest accuracy of 85.3 % was recorded by both SVM classifier with RBF kernel and the NBC classifier. However, a good classifier should give equally high values for sensitivity and specificity in studies such as this in order for the classifier to not be biased towards one class. In this angle, the SVM classifier is better than the NBC as it presents a sensitivity of 84.4 % and equally good specificity of 85.9 %.

The accuracy obtained for the UK dataset (85.3 %) is lower than that recorded for the Portugal dataset (93.1 %). A higher accuracy is difficult to achieve for the UK dataset for the following reason: all plaques are initially asymptomatic. In this cross-sectional study, when the dataset was collected, 196 plaques had already become symptomatic. Over time, some additional unstable plaques are likely to rupture and become symptomatic. According to their texture, such plaques would be classified by our algorithm as high risk and unstable although at the time of imaging they would be clinically asymptomatic. Hence, the accuracy is bound to be lower. This issue can only be resolved by prospective longitudinal studies. The Portugal dataset acquisition protocol, on the other hand, was designed to be a longitudinal study, and hence, the images were confirmed to be *Sym* or *Asym* after adequate follow-up. Therefore, the texture of the plaques adequately described the respective class without any ambiguity, and hence, the classifiers were able to perform with better accuracy.

Table 3 Classifier performance measures

Classifier	Portugal dataset				UK dataset			
	A	PPV	Sn	Sp	A	PPV	Sn	Sp
SVM: Linear	84	83.9	96	57.8	84.6	81.9	83	85.9
SVM: Poly 1	84	83.9	96	57.8	84.6	81.9	83	85.9
SVM: Poly 2	86.8	87.2	94.9	68.9	84	80.8	83	84.7
SVM: Poly 3	86.8	87.9	93.9	71.1	82.7	81.7	78.5	85.9
SVM: RBF	83.3	83.5	94.9	57.8	**85.3**	**82.3**	**84.4**	**85.9**
DT	76.4	81	85.9	55.6	79.2	76.5	74.8	82.5
Fuzzy	**93.1**	**91.8**	**99**	**80**	81.4	80	77	84.7
GMM	63.2	90.7	52.5	86.7	79.2	84.9	64.4	90.4
KNN	74.3	80	82.8	55.6	83.7	82.5	79.3	87
NBC	54.2	79.8	45.5	73.3	**85.3**	**84.5**	**81.5**	**88.1**

The highest accuracies obtained in each dataset are highlighted in bold

All values in %

A accuracy, *Sn* sensitivity, *Sp* specificity

6.3 Integrated indices

The ranges of *PlaqueIndexP* and *PlaqueIndexU* for both the *Sym* and *Asym* classes are presented in Table 4. It is evident that the both the indices have a significantly distinct range for the two classes. In the case of *PlaqueIndexP*, the asymptomatic images have a higher value which might probably be because of the presence of the most of the features that have higher values for the asymptomatic plaques in the numerator of (23). In the case of *PlaqueIndexU*, the symptomatic images have a higher value which might be because of the presence of the most of the features that have higher values for the symptomatic plaques in the numerator of (26).

7 Discussion

A review of the computerized methods used for plaque analysis can be found in Kyriacou et al. [26]. Christodoulou et al. [11] used 61 texture and shape features from 230 plaque ROIs in a modular neural network and obtained a classification accuracy of 73.1 %. Mougiakakou et al. [27] quantified plaque echogenicity characteristics using first-order statistical features and Laws' texture. On classification of 54 images in each class using 21 features in a novel hybrid neural network, they reported an accuracy of 99.1 %. Kyriacou et al. [24] used texture and morphological features in neural and statistical classifiers and reported an accuracy of around 71.2 % using 10 features. In 2009, the same group [25] employed multilevel binary and grayscale morphological analyses. Using pattern spectra features from 274 plaques in an SVM classifier, they reported an accuracy of 73.7 %. In 2009, Seabra et al. [34] extracted 114 features (based on morphological, histogram and Rayleigh parameters, and image texture) from plaques (102 *Asym* and 44 *Sym*). They obtained an accuracy of around 99.2 % using the Adaboost classifier. Previously [4], we evaluated a combination of 29 texture-based features, DoS, gray-scale mean, and P40 value extracted from 110 asymptomatic plaques and 50 symptomatic plaques

Table 4 Range of Clinical Indices

	Symptomatic	Asymptomatic	*p* value
PlaqueIndexP	0.94E+05 ± 0.00E+05	6.12E+05 ± 0.17E+05	<0.0001
PlaqueIndexU	5.06E+20 ± 0.14E+20	0.24E+20 ± 0.00E+20	<0.0001

and obtained a classification accuracy of 90.66 % using the SVM classifier.

In the studies summarized above, three issues are evident: (1) the number of features used for classification is voluminous increasing the computational time and complexity, (2) there is still room for improvement in accuracy, and (3) plaques are manually segmented leading to inter-observer variabilities and errors. In this work, we have addressed the first two issues, and developed CAD techniques that present adequate classification accuracy using a small feature set.

In our earlier experiments with the Portugal dataset [5], we extracted a combination of discrete wavelet transform, higher order spectra and textural features. On using these features in a SVM classifier with RBF kernel function, we observed an accuracy of 91.7 %. The accuracy obtained using the proposed system for the Portugal dataset is significantly higher (93.1 %) than the one we reported in [5] (91.7 %). In another earlier study [2], we extracted texture features alone (standard deviation, entropy, symmetry, and run percentage) from the UK dataset, and obtained an accuracy of 82.4 % using SVM with RBF kernel, which is lower than the accuracy obtained for this dataset in this study (85.3 %). Thus, the proposed novel combination of features does provide improved classification accuracies in both the datasets. The proposed techniques have the following features:

- They are low cost as (a) the commonly acquired ultrasound images are used, and (b) the algorithms can be easily written as a software application and installed at no cost.
- The system is real-time as no manual interaction is necessary except for the selection of the ROI. The ROI can be easily traced by expert ultrasonographers.
- The feature set is small (maximum of 17 features), and yet is powerful as indicated by the good classification results.
- Generalization and the robustness have been achieved because of the use of cross-validation technique.
- The proposed novel integrated indices can be valuable in objectively assessing the nature of the plaque and in monitoring plaque morphology changes.

Ultrasound system parameters such as frequency, aperture, pulse length, and non-linear post-processing techniques that are present in advanced systems that modify the texture of the acquired image will affect the values of the features extracted in this work. Our future studies will incorporate techniques to study this effect. We have shown that the ground truth plays a very important role in the success of classification. Even though the techniques present good accuracies, we intend to test them on more datasets in the future. The accuracy may be improved by evaluating other features such as fractal dimension which was found to be significantly different between the two classes [6]. We also intend to extend the technique to 3D characterization.

As highlighted previously, some asymptomatic plaques which are in the process of becoming symptomatic tend to have the textures typical of symptomatic plaques. In such cases, our classifiers will classify them as symptomatic when the ground truth is in effect asymptomatic. This is the reason for the lower accuracy of UK dataset as plaques were not monitored over long periods of time when this dataset was collected. However, in the case of the Portugal dataset, adequate monitoring was done to confidently determine the class label of the plaque. Hence, classifiers could give better accuracies. Moreover, some of the asymptomatic plaques might have been labeled as symptomatic when the symptoms might have occurred due to plaque in areas other than the carotid artery. Also, patients who do not recollect their history of symptoms may be classified as asymptomatic. Due to these reasons, future studies are necessary in which the ground truth of whether the studied carotid plaque is the reason for symptoms would be based on pathological studies on the plaque instead of on the patient's symptoms.

8 Conclusions

We have demonstrated that texture features and features based on the trace transform can adequately characterize the plaque tissue and thereby aid in classification of symptomatic and asymptomatic plaques with accuracies ranging to 93.1 and 85.3 %, respectively, for two different kinds of data sets. Since we employed stratified cross-validation method for evaluation of the proposed CAD techniques, the classifiers were evaluated using test images that were not included in the training set, and hence, are robust for analyzing new images. We have also proposed novel plaque indices which can more objectively differentiate between the two classes. Additional studies are needed in future to establish the robustness of the proposed techniques and the indices.

References

1. Aburahma AF, Thiele SP, Wulu JT Jr (2002) Prospective controlled study of the natural history of asymptomatic 60 % to 69 % carotid stenosis according to ultrasonic plaque morphology. J Vasc Surg 36(3):437–442
2. Acharya UR, Faust O, Alvin AP, Sree SV, Molinari F, Saba L, Nicolaides A, Suri JS (2011) Symptomatic vs. asymptomatic plaque classification in carotid ultrasound. J Med Syst. doi: 10.1007/s10916-010-9645-2
3. Acharya UR, Sree SV, Rama Krishnan MM, Molinari F, Saba L, Ho SY, Ahuja AT, Ho SC, Nicolaides A, Suri JS (2012) Atherosclerotic risk stratification strategy for carotid arteries using texture-based features. Ultrasound Med Biol 38:899–915
4. Acharya UR, Rama Krishnan MM, Sree SV, Sanches J, Shafique S, Nicolaides A, Pedro LM, Suri JS (2012) Plaque tissue characterization and classification in 2D ultrasound longitudinal carotid scans: a paradigm for vascular feature amalgamation. IEEE Trans Instrum Meas (in press)
5. Acharya UR, Faust O, Sree SV, Alvin APC, Krishnamurthi G, Seabra JCR, Sanches J, Suri JS (2012) Understanding symptomatology of atherosclerotic plaque by image-based tissue characterization. Comput Meth Prog Bio. doi:10.1016/j.cmpb.2012.09.008 (in press)
6. Asvestas P, Golemati S, Matsopoulos GK, Nikita KS, Nicolaides AN (2002) Fractal dimension estimation of carotid atherosclerotic plaques from B-mode ultrasound: a pilot study. Ultrasound Med Biol 28(9):1129–1136
7. Box JF (1987) Guinness, gosset, fisher, and small samples. Statist Sci 2(1):45–52
8. Brott TG, Hobson RW 2nd, Howard G, Roubin GS, Clark WM, Brooks W, Mackey A, Hill MD, Leimgruber PP, Sheffet AJ, Howard VJ, Moore WS, Voeks JH, Hopkins LN, Cutlip DE, Cohen DJ, Popma JJ, Ferguson RD, Cohen SN, Blackshear JL, Silver FL, Mohr JP, Lal BK, Meschia JF, CREST Investigators (2010) Stenting versus endarterectomy for treatment of carotid-artery stenosis. N Engl J Med 363(1):11–23
9. Carr S, Farb A, Pearce WH, Virmani R, Yao JS (1996) Atherosclerotic plaque rupture in symptomatic carotid artery stenosis. J Vasc Surg 23(5):755–765
10. Carter-Monroe N, Yazdani SK, Ladich E, Kolodgie FD, Virmani R (2011) Introduction to the pathology of carotid atherosclerosis: histologic classification and imaging correlation. In: Suri JS, Kathuria C, Molinari F (eds) Atherosclerosis disease management. Springer, New York, pp 3–35
11. Christodoulou CI, Pattichis CS, Pantziaris M, Nicolaides A (2003) Texture based classification of atherosclerotic carotid plaques. IEEE Trans Med Imaging 22(7):902–912
12. David V, Sanchez A (2003) Advanced support vector machines and kernel methods. Neurocomputing 55(1–2):5–20
13. Elatrozy T, Nicolaides A, Tegos T, Griffin M (1998) The objective characterization of ultrasonic carotid plaque features. Eur J Vasc Endovasc Surg 16(3):223–230
14. Elmore JG, Armstrong K, Lehman CD, Fletcher SW (2005) Screening for breast cancer. JAMA 293(10):1245–1256
15. European Carotid Surgery Trialists' Collaborative Group (1998) Randomized trial of endarterectomy for recently symptomatic carotid stenosis: final results of the MRC European Carotid Surgery Trial (ECST). Lancet 351(9113):1379–1387
16. Gaitini D, Soudack M (2005) Diagnosing carotid stenosis by Doppler sonography: state of the art. J Ultrasound Med 24(8):1127–1136
17. Galloway MM (1975) Texture analysis using gray level run lengths. Comput Graph Image Process 4(2):172–179
18. Golemati S, Tegos TJ, Sassano A, Nikita KS, Nicolaides AN (2004) Echogenicity of B-mode sonographic images of the carotid artery: work in progress. J Ultrasound Med 23(5):659–669
19. Griffin M, Kyriakou E, Nicolaides A (2007) Normalization of ultrasonic images of atherosclerotic plaques and reproducibility of gray-scale media using dedicated software. Int Angiol 26(4):372–377
20. Han J, Kamber M, Pei J (eds) (2005) Data mining: concepts and techniques. Morgan Kaufmann, USA
21. Inzitari D, Eliasziw M, Gates P, Sharpe BL, Chan RK, Meldrum HE, Barnett HJ (2000) The causes and risk of stroke in patients with asymptomatic internal-carotid-artery stenosis. North American Symptomatic Carotid Endarterectomy Trial Collaborators. N Engl J Med 342(23):693–700
22. Jawahar CV, Ray AK (1996) Incorporation of gray-level imprecision in representation and processing of digital images. Pattern Recogn Lett 17(5):541–546
23. Kadyrov A, Petrou M (2001) The trace transform and its applications. IEEE Trans Pattern Anal Mach Intel 23(8):811–828
24. Kyriacou E, Pattichis MS, Christodoulou CI, Pattichis CS, Kakkos S, Griffin M, Nicolaides A (2005) Ultrasound imaging in the analysis of carotid plaque morphology for the assessment of stroke. Stud Health Technol Inform 113:241–275
25. Kyriacou E, Pattichis M, Pattichis CS, Mavrommatis A, Christodoulou CI, Kakkos S, Nicolaides A (2009) Classification of atherosclerotic carotid plaques using morphological analysis on ultrasound images. J Appl Intell 30(1):3–23
26. Kyriacou EC, Pattichis C, Pattichis M, Loizou C, Christodoulou C, Kakkos SK, Nicolaides A (2010) A review of noninvasive ultrasound image processing methods in the analysis of carotid plaque morphology for the assessment of stroke risk. IEEE Trans Inf Technol Biomed 14(4):1027–1038
27. Mougiakakou SG, Golemati S, Gousias I, Nicolaides AN, Nikita KS (2007) Computer-aided diagnosis of carotid atherosclerosis based on ultrasound image statistics, laws' texture and neural networks. Ultrasound Med Biol 33(1):26–36
28. Muller KR, Mika S, Ratsch G, Tsuda K, Scholkopf B (2001) An introduction to kernel based learning algorithms. IEEE Trans Neural Networks 12(2):181–201
29. Polak JF, Shemanski L, O'Leary DH, Lefkowitz D, Price TR, Savage PJ, Brant WE, Reid C (1998) Hypoechoic plaque at US of the carotid artery: an independent risk factor for incident stroke in adults aged 65 years or older. Cardiovascular Health Study. Radiology 208(3):649–654
30. Rocha R, Silva J, Campilho A (2012) Automatic segmentation of carotid b-mode images using fuzzy classification. Med Biol Eng Comput 50:533–545
31. Ross TJ (ed) (2004) Fuzzy logic with engineering applications. Wiley, West Sussex
32. Rossi AC, Brands PJ, Hoeks AP (2010) Automatic localization of intimal and adventitial carotid artery layers with noninvasive ultrasound: a novel algorithm providing scan quality control. Ultrasound Med Biol 36(3):467–479
33. Rothwell PM, Gutnikov SA, Warlow CP, European Carotid Surgery Trialist's Collaboration (2003) Reanalysis of the final results of the European Carotid Surgery Trial. Stroke 34(2):514–523
34. Seabra J, Pedro LM, e Fernandes F, Sanches J (2010) Ultrasonographic characterization and identification of symptomatic carotid plaques. In: Engineering in Medicine and Biology Society, 2010. EMBS 2010. 32th Annual International Conference of the IEEE, pp 6110–6113
35. Sugeno M (ed) (1985) Industrial applications of fuzzy control. Elsevier, Amsterdam

36. Suri JS, Kathuria C, Molinari F (eds) (2011) Atherosclerosis disease management. Springer, New York
37. Tomita F, Tsuji S (1990) Computer analysis of visual textures. Kluwer Academic Publishers, Boston
38. Weszka JS, Rosenfield A (1976) An application of texture analysis to material inspection. Pattern Recogn 8(4):195–200
39. World Health Organization, CVD (2012). http://www.who.int/mediacentre/factsheets/fs317/en/index.html